


Clogging of granular materials in a horizontal hopper: Effect of outlet size, hopper angle, and driving velocity

Quan-Chun Yu, Ning Zheng ^{*}, and Qing-Fan Shi[†]

School of Physics, Beijing Institute of Technology, Beijing 100081, China



(Received 3 March 2021; accepted 29 April 2021; published 17 May 2021)

Due to the independence of the driving velocity and outlet size, it is possible to isolate geometrical and kinematic contributions to clogging in two-dimensional horizontal flow in a hopper driven by a conveyor belt. We experimentally investigate the geometric (outlet size and hopper angle) and kinematic effects (driving velocity) on the clogging in such a horizontal flow. Based on quantitative measurements and analysis of the avalanche size, blocking probability of a particle at the outlet, and other parameters, we show that the geometric factors can more effectively affect clogging. In addition, we find that the clogging tends to be alleviated with the increases of the driving velocity, suggesting a possible “fast is fast” behavior within a wide range of driving velocity. We borrow and modify a model from clogging in gravity-driven hoppers, which can accurately describe the shape of the clogging probability function in the conveyor belt driven flow, suggesting that these two systems could share some mechanisms for clogging.

DOI: [10.1103/PhysRevE.103.052902](https://doi.org/10.1103/PhysRevE.103.052902)

I. INTRODUCTION

Clogging and flowing behavior of discrete materials through a bottleneck are ubiquitous in many systems across several scales: crowd evacuation [1], hopper flow [2], thrombus in vascular stenosis [3], and microparticles’ agglomeration in constraint [4]. Clogging is sometimes beneficial, such as blood clotting of wounds, and accelerated proliferation of cells in crowded spaces. However, clogging also causes serious issues: traffic bottlenecks on poorly designed roads bring huge economic losses each year; the blockage of materials in industrial hoppers leads to production interruption and even casualties. It is of great social and economic significance to study the passage of a many-particle system through a bottleneck.

Clogging in hopper flow is a typical bottleneck clogging phenomenon, and many fruitful studies have shed light on the way in which clogging is influenced by outlet size [2,5], outlet shape [6,7], particle shape [8,9], particle deformability and friction [10], the presence of obstacles [11–13], and interstitial media [14,15]. However, most studies on hopper or silo clogging have dealt with the case of particles purely discharged by gravity so far. Surprisingly, clogging in horizontal flow has not attracted much attention yet, although this class of clogging is ubiquitous and of fundamental importance in industry and human society, such as clogging in conveyor belt flow, traffic flow, and pedestrian flow.

In previous studies on clogging in gravity-driven hopper flow, it has been found that the formation of clogging is due to the arching of particles in front of an outlet. The development and stability of arching are closely related to the outlet size

and particle velocity before the outlet. The outlet size reflects the geometric contribution on clogging. The wider an outlet is, the more difficult forming an arch is. The particle velocity near an outlet represents the kinematic contribution to hopper clogging. The larger the velocity is, the less likely the fast-moving particles stably form an arch due to the large kinetic energy of particles at the outlet.

Unfortunately, it is very difficult to isolate the two contributions on hopper or silo clogging in a gravity discharged system, in which the particle velocity scales with $v \propto \sqrt{gR}$, and thus the flow rate $Q \propto \sqrt{g}(2R - kd)^{3/2}$, where R is the radius of the outlet, d is particle diameter, and g is the gravity acceleration. The outlet size couples with the particle velocity, and the change of the outlet size results in the simultaneous variation of the particle velocity. Because of this challenge, there are few studies on the independent contribution of the two effects on clogging in a gravity discharged hopper. In these efforts, tuning the system’s effective gravity is a common but slightly indirect method [16,17]. Recently, Gella *et al.* came up with an ingenious way to decouple the particle velocity from the outlet size in the gravity discharged silo by placing a conveyor belt beneath the outlet of a silo, and investigated the independent contribution from the two effects to the clogging process [18].

In contrast to the gravity-driven hopper flow, the horizontal conveyor belt flow allows control of the particle velocity independent from the outlet size. In the case of the conveyor belt, the empirical law for the flow rate is $Q = C \frac{V}{d} (\frac{D_0}{d} - k)$, showing the independent relation between the driving velocity and the outlet size, where V is the driving velocity of the conveyor belt, and D_0 is the outlet size [19]. The decoupling is suitable for exploring the independent contributions of geometry and kinematics to clogging in horizontal flow. Furthermore, it is also an interesting question whether the clogging in a gravity-driven hopper and conveyor belt hopper system share the same

^{*}ningzheng@bit.edu.cn

[†]qfshi123@bit.edu.cn

or similar physical laws, although the two systems seem quite different.

In this work, we experimentally investigate the effects of the outlet size, hopper angle, and driving belt velocity on clogging characteristics of granular particles through a bottleneck on a conveyor belt. Here we use several parameters, such as avalanche size and clogging probability, to describe the clogging process. We demonstrate that a model for the gravity-driven hopper clogging can well describe the dependence of the clogging probability on the outlet size in conveyor belt hopper flow. Based on this model, we propose a modified model which predicts the relationship between the clogging probability and hopper angle. Through quantitative comparison and analysis of the experimental results, we discuss the extent of the geometrical contribution (outlet size and hopper angle) and kinematic contribution (driving velocity) on clogging. Finally, a possible “fast is fast” behavior is found in the conveyor belt system.

II. EXPERIMENTAL SETUP

The flowing and clogging behavior of granular particles driven by a two-dimensional conveyor belt as they pass through a bottleneck is experimentally investigated. A circulation conveyor belt is used to continuously supplement the particles in the upstream granular flow, maintaining a basically constant number of particles before the narrow outlet, and improving the efficiency of data acquisition as well, as shown in Fig. 1(a). An acrylic plate covers the conveyor belt, and the gap between the plate and the conveyor belt is slightly wider than the particle thickness (the particles used in the experiment are disks with a diameter of 11 mm and a thickness of 4.5 mm). Therefore, only a monolayer of particles is allowed between the acrylic plate and the conveyor belt, and the flowing system is a two-dimensional system.

The width of the conveyor belt is 440 mm, more than 30 times a particle diameter. Therefore, the effect of side walls on the granular flow can be ignored. Two wedge baffles are placed opposite each other at the lower end of the acrylic plate to form a narrow outlet [see Fig. 1(b)]. The wedge outlet is chosen to prevent particles from forming an arch on the side wall of the baffle. By adjusting the length of the wedge baffle, different outlet sizes can be conveniently obtained, and the outlet width is D_0 . Here, the particle diameter d is used to normalize the outlet width, $D = D_0/d$. In addition, different hopper angles, θ , can be obtained by tuning the walls on the wedge baffles, as shown in Fig. 1(c).

About 2000 Plexiglas disk particles are used in the experiment. These particles passing through an outlet are driven by a conveyor belt. If the outlet size is small, the particles will arch before the outlet spontaneously [see Fig. 1(b)], resulting in clogging, i.e., flow interruption. The clogging in the horizontal hopper flow driven by a conveyor belt is markedly different from that in the gravity-driven granular hopper flow. The latter is extremely difficult to unclog spontaneously once the arch is formed, and the clogging status will persist until the arch is broken by external disturbance. In contrast, spontaneous unclogging often occurs in horizontal flow due to the continuous shear on the arch by the conveyor belt. Therefore, intermittent flow is more common, as shown in Fig. 1(d). The plateaus in

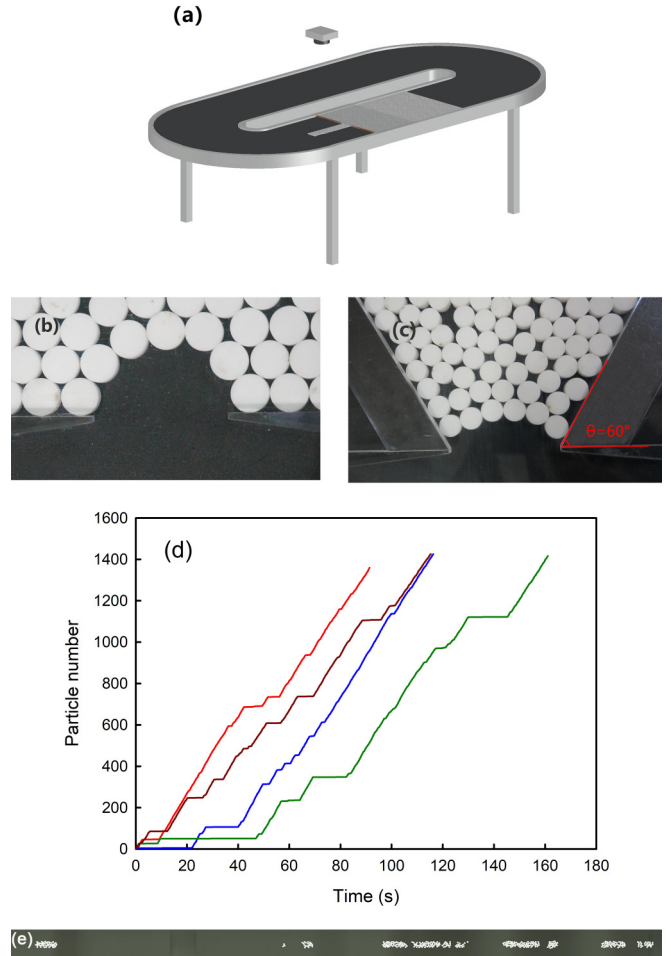


FIG. 1. (a) Sketch of the experimental setup. (b) Wedge outlet. (c) Hopper angle θ . The hopper angle can be adjusted from $\theta = 0^\circ$ (flat-bottom hopper) to $\theta = 90^\circ$ (pipeline hopper). (d) Representative curves of the number of particles crossing the outlet as a function of time; plateaus in the curve indicate the development of clogging. Each line corresponds to an independent trial. (e) A spatiotemporal diagram of the disk particles as they discharge out of the outlet.

time evolution curves indicate clogging status. For situations of persistent clogging, after 200 s, if the system still fails to resume flow spontaneously, a jet of compressed air aimed at the outlet is blown to break the arch and the flow is restored.

We use a camera (720×1280 pixels at 25 frames/s) to record discharging of each particle out of the outlet. An image, such as the one shown in Fig. 1(e), is constructed from the video in the following way. We first define an image sampling window downstream near the outlet. The width of the sampling window is about twice the width of the outlet, and the length of the window is equal to the displacement of the particles passing through the outlet within one frame time of the camera. We extract an image within the sampling window from each frame, and stack the sampling images in sequence to form the spatiotemporal diagram which describes the relative position of every particle passing through the outlet. The vertical dimension in this spatiotemporal diagram is the distance along the width of the sampling window, and the horizontal dimension represents the time, in units of the

sampling period. Next, an image recognition algorithm is used to extract the y coordinate (the y direction is the direction of the driving velocity) of each particle in the spatiotemporal diagram, calculate the spatial interval between the passage of consecutive particles, and obtain the time lapse of consecutive particles with the driving velocity of the conveyor belt. The time lapse is further processed to obtain important information, such as an appropriate clogging time lapse to determine a clogging event and avalanche size, presented in the subsequent sections.

III. EXPERIMENTAL RESULTS

A. Dependences of clogging and flowing statistics on the outlet size

This section focuses on the effect of the outlet size on the clogging, where the driving velocity of the conveyor belt is fixed at 8 cm/s and the hopper angle is 0° . Unlike the conventional gravity-driven hopper flow, horizontal hopper flow driven by a conveyor belt has difficulties in defining a clogging event. This is because the conveyor belt continuously destabilizes the clogging arch through cyclic shear, leading to random occurrences of spontaneous unclogging. This results in a huge fluctuation of clogging time interval, from 1 s to more than 100 s. Therefore, it is difficult to select an appropriate clogging time interval to define a clogging event. Such a problem of how to define clogging events has also appeared in the clogging of sheep and other active particles passing through a bottleneck, and has been properly solved [20,21].

As mentioned previously, the time lapse Δt between the passage of consecutive particles is extracted, and the complementary cumulative distribution function (CCDF) of the time lapse is obtained; see Fig. 2(a). The distribution function has a power-law tail, $P(t \geq \Delta t) \propto \Delta t^{1-\alpha}$, as observed in other systems such as sheep, pedestrians, and gravity-driven hopper flow [20–23]. Here we use a rigorous method (the Clauset-Shalizi-Newman method) to fit the CCDF, and obtain the exponent of a power-law tail α , and the minimum time lapse Δt_c , in seconds, from which the fit is valid [24].

The exponent of a power-law tail has been used to speculate whether a system possibly tends to flow or clog [20,22]. When $\alpha \leq 2$, the system could be prone to clogging. Otherwise, the system could be inclined to flow. The experimental measurement seems to be consistent with this statement. In Fig. 2(a), when the outlet size $D < 5.5$, the power-law exponent α is less than 2 and the system tends to clog. When the outlet size $D > 5.5$, the power-law exponent α is larger than 2 and particles continuously flow out of the outlet almost without any interruption. The minimum time lapse Δt_c is used to define clogging events. Once Δt_c is chosen, the passage of particles can be considered as “flowing” if $\Delta t < \Delta t_c$, and “clogging” if $\Delta t \geq \Delta t_c$. The values of Δt_c are about 0.1–0.3 s for different outlet sizes. Two parameters, α and Δt_c , are shown in Table I.

Additionally, there is another approach to estimate Δt_c [20]. In this method we need to calculate the mean flow rate within the avalanches. Here, the mean flow rate is defined as follows: We take the avalanche size (namely, the particle number between two consecutive clogging events) divided by

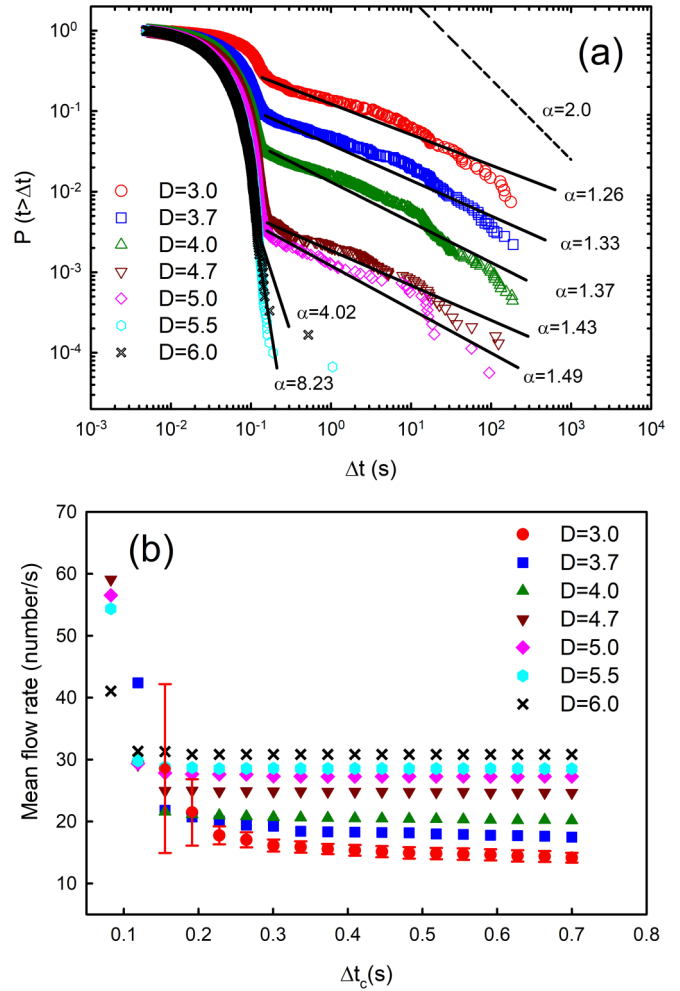


FIG. 2. (a) Time-lapse CCDFs obtained from different outlet sizes. The solid lines represent the power-law fits with exponent α . The dashed line marked with $\alpha = 2.0$ is the dividing line between a clogging and flowing regime. (b) The mean flow rate as a function of Δt_c . For clarity, error bars only show in a single curve. Other curves have similar error bars.

the avalanche duration (the time between two clogging events) for all the avalanches, and calculate the weighted average. The weight of an avalanche size is the ratio of the avalanche size to the total number of particles. As Δt_c decreases, the avalanche size becomes smaller correspondingly, because the

TABLE I. Values of two parameters for the different outlet sizes. α is the exponent of the power-law tail, and Δt_c is the value of the minimum time lapse above which the fit is valid.

| Outlet size D | Power-law exponent α | Δt_c (s) |
|-----------------|-----------------------------|------------------|
| 3 | 1.26 | 0.30 |
| 3.7 | 1.33 | 0.20 |
| 4 | 1.37 | 0.20 |
| 4.7 | 1.43 | 0.20 |
| 5 | 1.49 | 0.20 |
| 5.5 | 4.02 | 0.15 |
| 6 | 8.23 | 0.10 |

shorter time lapses are considered clogs. The granular flow is divided into more avalanche sizes, and the mean flow rate necessarily increases. As can be seen in Fig. 2(b), when $D = 6.0$, the mean flow rate tends to be stable at $\Delta t_c = 0.1$ s; when $D = 3.0$, the mean flow rate saturates at $\Delta t_c = 0.3$ s. For the rest of the outlet sizes, the mean flow rate quickly approaches a stable flow rate after $\Delta t_c = 0.2$ s. The value range of $\Delta t_c = 0.1-0.3$ s is almost the same as that obtained with the Clauset-Shalizi-Newman method. Thus, the two methods can be cross tested to acquire reliable Δt_c . In our analysis, the minimum time lapse used to set apart avalanches is 0.3 s. Although the choice influences the value of mean avalanche size $\langle s \rangle$, the exponential tail of the avalanche size distribution is unaffected.

We can define some physical quantities to characterize flowing and clogging in the system. The avalanche size s , namely, the particle number between two consecutive clogging events, is an important parameter in the flowing regime. We can obtain the avalanche size distribution for each outlet and the corresponding average avalanche size $\langle s \rangle$. By defining a rescaled avalanche size $s^* = s/\langle s \rangle$, we find that the rescaled avalanche sizes overlap to form a single curve with an exponential tail, as shown in Fig. 3(a). Notably, the same exponential tail also exists in sheep or pedestrians passing through a narrow gate and in the discharging of a gravity-driven hopper flow [20,23,25].

With the avalanche size, we can introduce clogging probability J as the probability that flow gets stopped before N particles pass through the outlet [26]. $J_N(D) = 1 - \sum_{s=N}^{\infty} n_D(s)$, where $n_D(s)$ is the probability of an avalanche size of s particles. According to the definition, the physical implication of the J is the probability that the avalanche size is smaller than N . In other words, J gives the clogging probability before N particles flow out of a given outlet, which depends on the N and system parameters such as the outlet size D and driving velocity V_{belt} .

Figure 3(b) shows the dependence of clogging probability on the outlet size under different N . It can clearly be seen that the clogging probability $J_N(D)$ is nearly 1 for all N for a small outlet size $D < 2.5$, which indicates that the system is extremely prone to clogging with $D < 2.5$. When the outlet size $D > 6.5$, $J_N(D)$ approximately vanishes for all N , confirming that the flow is very unlikely to be arrested for a wide outlet. The curve shape is similar to the clogging probability curves in gravity-driven hopper flow [26,27].

In the clogging in two-dimensional gravity-driven hopper flow, Janda *et al.* proposed a model to describe the exponential decay of $n_D(s)$ for large avalanche size s [26]: $n_D(s) = p^s(1-p)$, and $1-p = A \exp(-B\eta^2)$, where p is the probability that a particle passes through an outlet without resulting in a blocking arch with adjacent particles; η is the number of particles that forms a blocking arch; A and B are fitting parameters. Based on the two equations above, the average avalanche size $\langle s \rangle$ can be obtained: $\langle s \rangle = A^{-1} \exp[B(\eta_0 D)^2] - 1$, where it is assumed that η is linearly proportional to the outlet size D , i.e., $\eta = \eta_0 D$, and η_0 is a fitting parameter.

Extending the model for a two-dimensional gravity-driven hopper clogging to a two-dimensional conveyor belt driven horizontal hopper flow, we can obtain the dependence of the average avalanche size $\langle s \rangle$ on the outlet size D ; see Fig. 4.

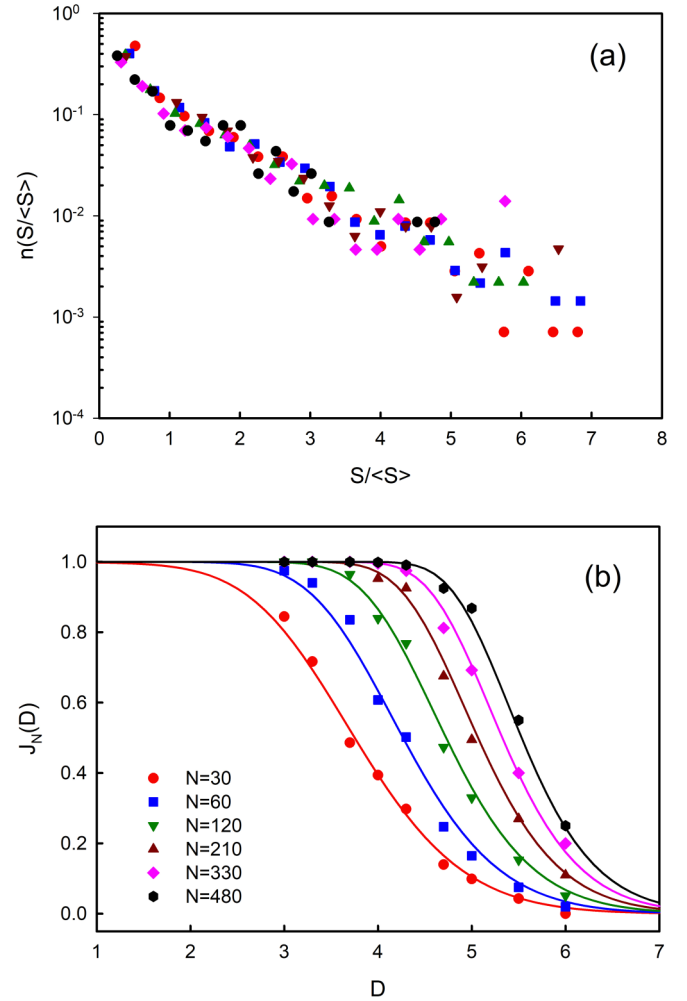


FIG. 3. (a) Rescaled probability density function of the avalanche size for different outlet sizes ($V_{\text{belt}} = 8$ cm/s, $\theta = 0^\circ$), as indicated in the legend in Fig. 2. (b) Clogging probability $J_N(D)$ as a function of the outlet size D . The fitted curves in the figure are given by Eq. (1).

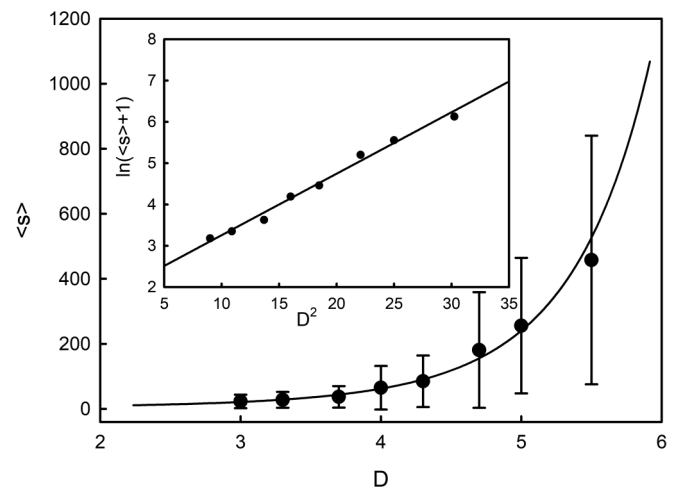


FIG. 4. The average avalanche size as a function of the outlet size. The solid line is the fit from $\langle s \rangle = A^{-1} \exp[B(\eta_0 D)^2] - 1$. The fitting parameters are $A^{-1} = 5.85$, $B\eta_0^2 = 0.149$. In the inset the plot of $\ln(\langle s \rangle + 1)$ vs D^2 shows the goodness of the fit.

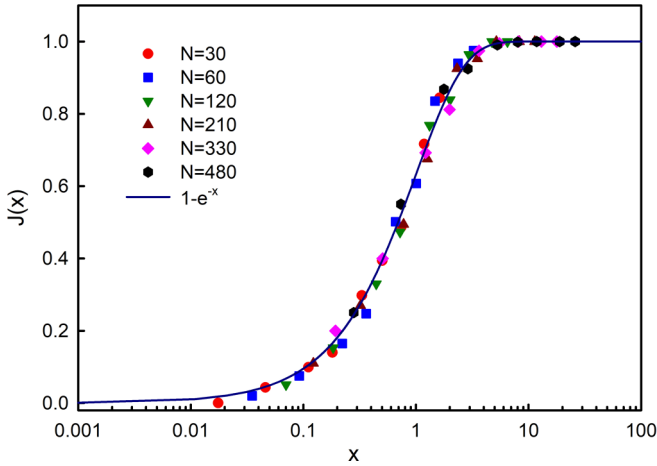


FIG. 5. The clogging probability J as a function of the rescaled variable $x = NAe^{-B(\eta_0 D)^2}$. The solid line corresponds to the function $1 - e^{-x}$.

In Fig. 4, the average avalanche size grows rapidly with the increase of D , and the experimental results are in good accord with the theoretical model $\langle s \rangle = A^{-1} \exp[B(\eta_0 D)^2] - 1$.

Inserting $\langle s \rangle = A^{-1} \exp[B(\eta_0 D)^2] - 1$ into $J_N(D) = 1 - \exp(-N/\langle s \rangle)$, we will have for $\langle s \rangle \gg 1$, that is, $\langle s \rangle \approx A^{-1} \exp[B(\eta_0 D)^2]$,

$$J_N(D) = 1 - \exp[-NAe^{-B(\eta_0 D)^2}]. \quad (1)$$

The solid lines in Fig. 3(b) are the theoretical results presented in Eq. (1), where A and $B\eta_0^2$ are fitting parameters obtained from the fit of $\langle s \rangle = A^{-1} \exp[B(\eta_0 D)^2] - 1$ to the data in Fig. 4. The experimental data agree with the theoretical results very well. We continue to define a variable $x = NAe^{-B(\eta_0 D)^2}$, and find that all data points from different N and D collapse onto a single curve which is the function $1 - e^{-x}$, as shown in Fig. 5. This agreement between the experimental data and theoretical prediction confirms that the model from the gravity-driven hopper clogging is also applicable to the relationship between clogging characteristics and outlet size in the conveyor belt driven horizontal hopper flow. This similarity implies that the clogging issues in the two systems could share some common physical laws. In addition, we investigate the relationship between the blocking probability of a particle near the outlet $1-p$ and the outlet size D , $\langle s \rangle = \frac{p}{1-p}$. Figure 6 manifests that $1-p$ decreases significantly with the increase of the outlet size D . The blocking probability $1-p$ for $D = 3.0$ is 20 times higher than that for $D = 5.5$.

B. Dependence of clogging and flowing statistics on the hopper angle

The hopper angle θ plays an important role in the transition between clogging and flowing. When the hopper angle reaches 90° , the granular flow becomes pipeline flow. For pipeline flow, clogging is hardly ever observed provided the pipeline width is larger than a few particle diameters. This is proved in our experiment: For pipeline flow with $D = 4.3$, particles continuously flow without clogging. However, for a flat bottom hopper ($\theta = 0^\circ$), clogging frequently occurs with

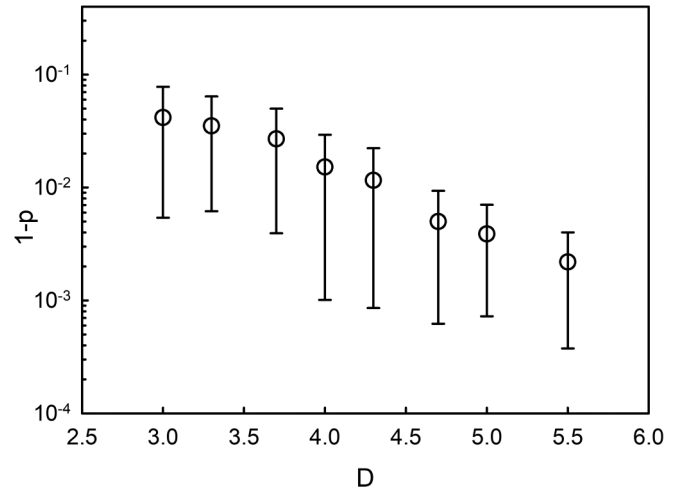


FIG. 6. Blocking probability that a particle clogs the outlet, $1-p$, vs the outlet size D .

the same outlet width. Therefore, a clogging-flowing transition should exist when the hopper angle varies from 0° to 90° . Recently, López-Rodríguez *et al.* investigated the role of the hopper angle in the transition between clogging and flowing in gravity-driven hopper flow, and indeed saw the trend of the transition. The probability of clogging can be reduced by three orders of magnitude with increasing hopper angle [28].

Using the same method described above, we obtain the complementary cumulative distribution function (CCDF) of the time lapse for different hopper angles. Figure 7(a) clearly shows that the power-law exponent increases with hopper angle, but the granular flow does not completely change into continuous flow until the hopper angle is 80° ($\alpha = 2.01$). As $\theta = 90^\circ$, pipeline flow appears with $\alpha = 9.86$, which further confirms that the pipeline flow is hardly interrupted. Figure 7(b) is still used to assist in determining the minimum time lapse Δt_c . With Δt_c obtained in Figs. 7(a) and 7(b), we adopt 0.3 s as Δt_c in this section.

Figure 8(a) shows that all rescaled avalanche size distributions collapse into a single exponential curve. Figure 8(b) shows the clogging probability $J_N(\theta)$ for different values of N with hopper angles ranging from $\theta = 0^\circ$ to $\theta = 90^\circ$. The clogging probability decreases as the hopper angle increases.

In previous work on the quantitative relationship between the hopper angle and the flow rate of particles discharging through an outlet, the hopper angle is considered to be related to an “acceleration region” above the outlet. For a flat-bottomed hopper ($\theta = 0^\circ$), the region is delineated by an arch with a radius of curvature $D/2$, corresponding to the convergence of the velocity stream through the outlet; for a hopper with a finite hopper angle, the radius of the arch is modified as $D/2 \cos \theta$ [29,30]. The avalanche size is the number of particles between two consecutive clogging events, which is closely related to flow rate. We conjecture that the equation to describe the relation between the average avalanche size and the outlet size $\langle s \rangle = A^{-1} \exp[B(\eta_0 D)^2] - 1$ for a flat-bottomed hopper ($\theta = 0^\circ$) may be extended to Eq. (2).

$$\langle s \rangle = A^{-1} \exp[B(\eta_0 D / \cos \theta)^2] - 1. \quad (2)$$

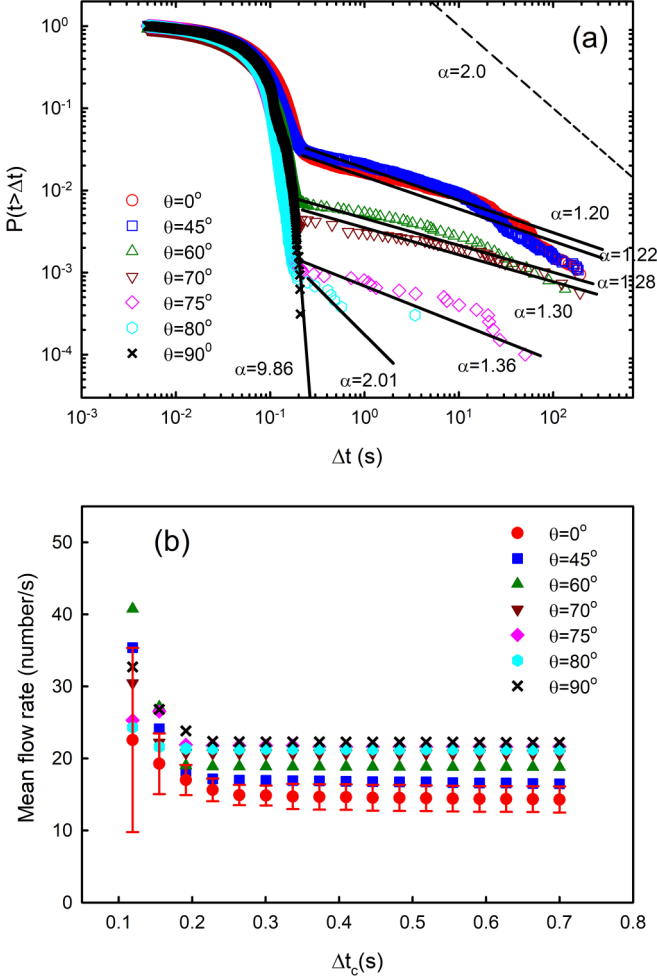


FIG. 7. (a) Complementary cumulative distribution function of the time lapse between passage of consecutive particles for different hopper angles ($D = 4.3$, $V_{\text{belt}} = 5$ cm/s). The solid lines represent fitting lines obtained by the Clauset-Shalizi-Newman method, and the corresponding power-law exponents are marked. The dashed line marked with $\alpha = 2.0$ is the dividing line between a clogging and a flowing regime. (b) The mean flow rate as a function of Δt_c for different hopper angles. For clarity, error bars are only shown in a single curve. Other curves have error bars with a similar size.

In Fig. 9, $\langle s \rangle$ grows rapidly as θ increases, and the experimental data are consistent with Eq. (2). The linear fit in the inset of Fig. 9 also confirms the validity of the modified equation. As before, we insert Eq. (2) into $J_N(D) = 1 - \exp(-N/\langle s \rangle)$. For $\langle s \rangle \gg 1$, $\langle s \rangle \approx A^{-1} \exp[B(\eta_0 D / \cos \theta)^2]$, we have

$$J_N(D, \theta) = 1 - \exp[-NAe^{-B(\eta_0 D / \cos \theta)^2}]. \quad (3)$$

The solid lines in Fig. 8(b) are theoretical results given by Eq. (3), where $A^{-1} = 42.19$; $B\eta_0^2 = 8.18 \times 10^{-4}$ are obtained from the fit of Eq. (2) to the data shown in Fig. 9. Furthermore, all data points cluster together to result in a single curve with a rescaled variable $x = NAe^{-B(\eta_0 D / \cos \theta)^2}$, as shown in Fig. 10. This confirms that the modified equation

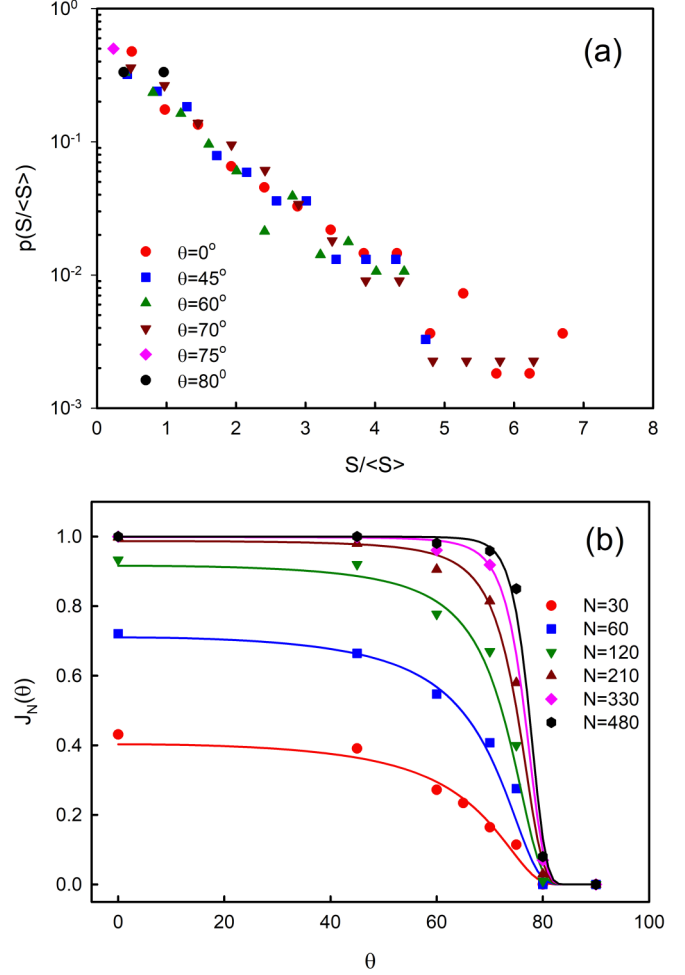


FIG. 8. (a) Rescaled probability density function of the avalanche size for different hopper angles ($D = 4.3$, $V_{\text{belt}} = 5$ cm/s), as indicated in the legend. (b) Clogging probability $J_N(\theta)$ as a function of the hopper angle. The fitted curves are given by Eq. (2).

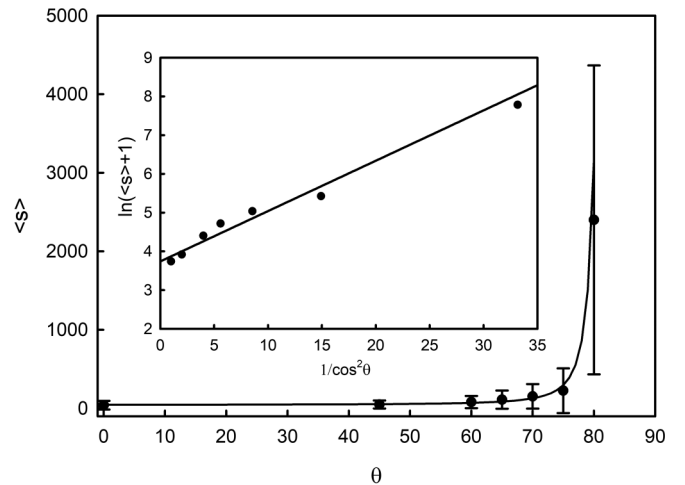


FIG. 9. Mean avalanche size as a function of a hopper angle ($D = 4.3$, $V_{\text{belt}} = 5$ cm/s). The solid line corresponds to the fit presented in Eq. (2), where the fitting parameters are $A^{-1} = 42.19$, $B\eta_0^2 = 8.18 \times 10^{-4}$. In the inset the linear fit between $\ln(\langle s \rangle + 1)$ and D^2 shows the goodness of the fit more clearly.

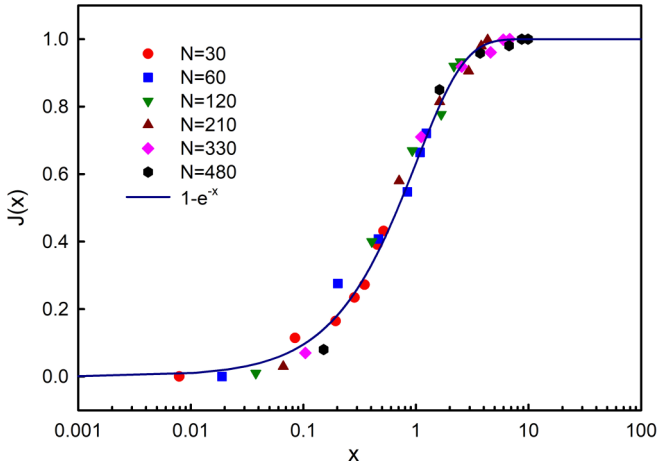


FIG. 10. The clogging probability J as a function of the rescaled variable $x = NAe^{-B(\eta_0 D / \cos \theta)^2}$. The experimental data for different hopper angles collapse into the theoretical curve predicted by Eq. (3).

can indeed describe the relationship between the clogging probability and the hopper angle.

When the hopper angle increases to $\theta = 80^\circ$, the blocking probability of a particle decreases more than 70 times, nearly two orders of magnitude, as shown in Fig. 11. With the further increase of the hopper angle, the time to measure the avalanche size is predicted to exceed the service time of the camera battery, so the experiment with hopper angle larger than 80° did not continue.

We speculate that the blocking probability of a particle at the outlet could continue to decrease with the increase of the hopper angle. In addition to the experimental extrapolation above, theoretical analysis gives a consistent conclusion. López-Rodríguez *et al.* have pointed out that the angle between adjacent frictionless particles constituting the clogging arch satisfies certain constraint conditions [28]: (1) All particle angles in the arch are within the range of $[90^\circ - \theta, -(90^\circ - \theta)]$, and $(90^\circ - \theta) \geq \theta_1 \geq \theta_2 \geq \theta_3 \dots \geq \theta_{n-1} \geq (-(90^\circ - \theta))$. (2) The shape of the arch is convex and the

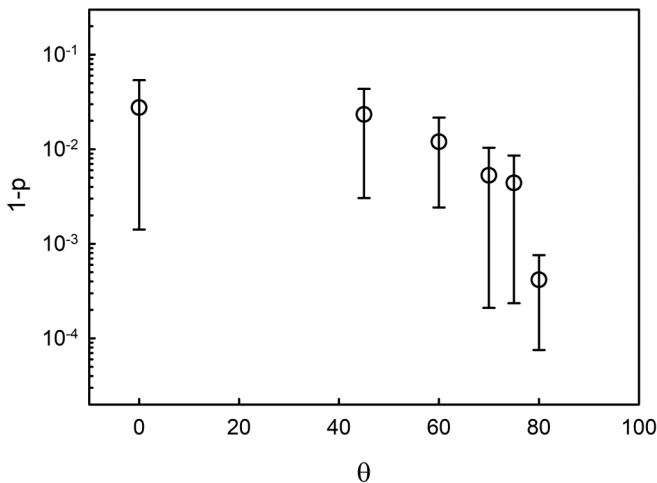


FIG. 11. The blocking probability of a particle at the outlet, $1-p$, as a function of the hopper angle ($D = 4.3$, $V_{\text{belt}} = 5 \text{ cm/s}$).

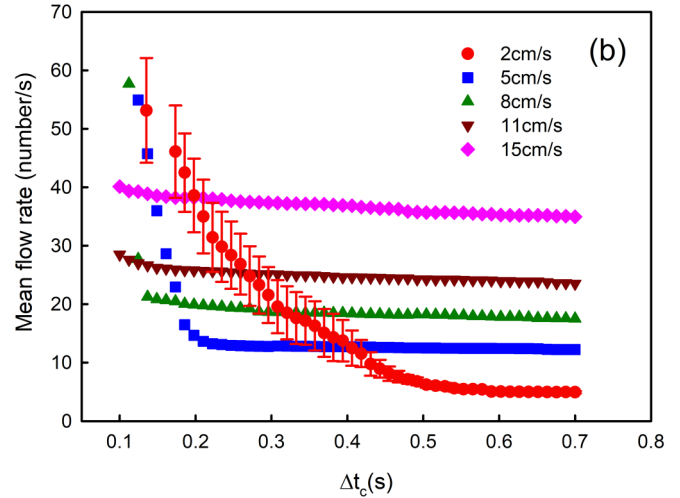
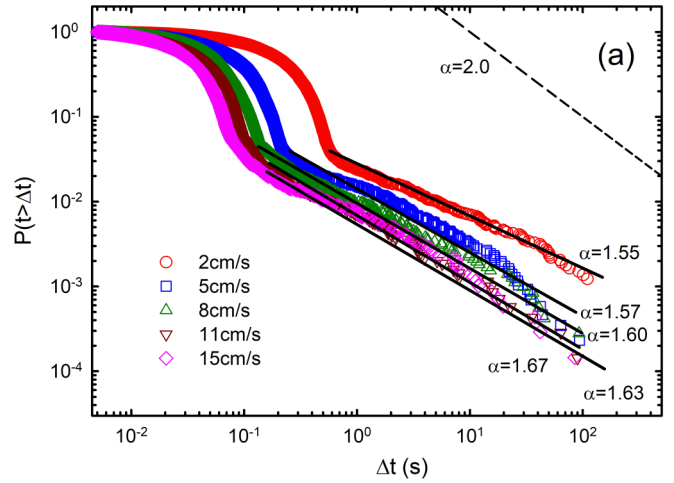


FIG. 12. (a) Time-lapse CCDFs obtained from different driving velocities ($D = 4.0$, and hopper angle $\theta = 0^\circ$). The solid lines represent the power-law fits with exponent α . (b) The mean flow rate as a function of Δt_c . For clarity, error bars are only shown in a single curve. Other curves have similar error bars.

span of the arch satisfies $[1 + (n-1) \cos(90^\circ - \theta)]d \leq l < nd$. When the particle flow is pipeline flow ($\theta = 90^\circ$), the angle range becomes $[0^\circ, 0^\circ]$, and the arch span cannot be larger than the outlet width, so the probability of particle clogging is very low for this case, or even zero. Moreover, according to Eq. (3), when the outlet size is a finite value and the hopper angle is 90° , it could be equivalent to expanding the outlet size to infinity, and thus the clogging probability J is very low. The results derived from the two theories are self-consistent. However, it is still an open question whether the blocking probability of a particle in a 90° hopper vanishes completely; this will be investigated in future work.

C. Dependence of clogging and flowing statistics on the driving velocity

In the past work of horizontal flow, it was found that the particle velocity is closely related to clogging. In particular, an increase of the velocity leads to more congestion of particles at the outlet, which is known as the “fast is slow” effect

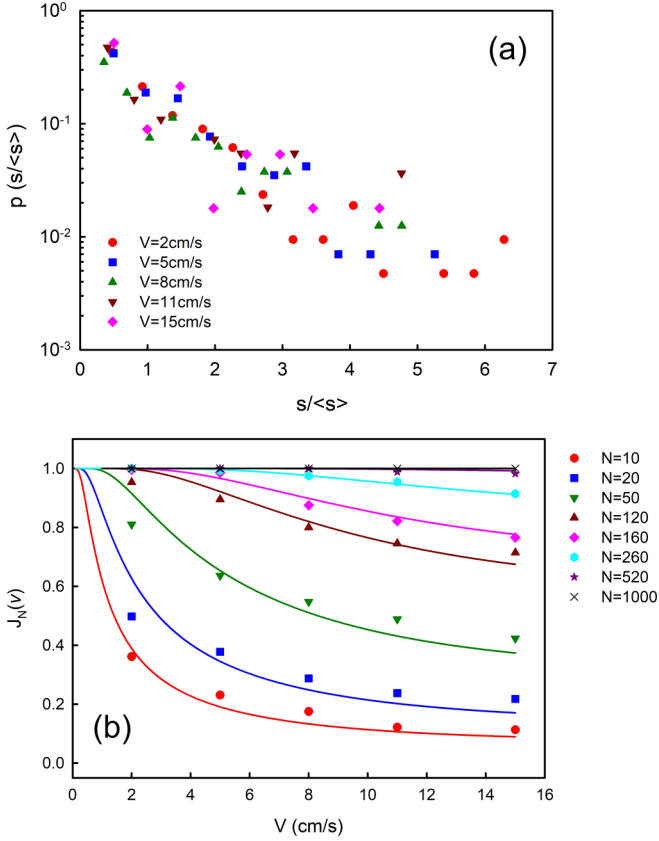


FIG. 13. (a) Rescaled probability density function of the avalanche size for different driving velocities ($D = 4.0$, $\theta = 0^\circ$), as indicated in the legend. (b) Clogging probability $J_N(v)$ as a function of the driving velocity V_{belt} . The fitted curves in the figure are given by Eq. (4).

[1,23,31,32]. Whether the same effect exists in the conveyor system remains elusive.

In this section, we fix the outlet size $D = 4.0$, hopper angle $\theta = 0^\circ$, and control the driving velocity of the conveyor belt V_{belt} from 2 to 15 cm/s. Using the same method described in previous sections, we obtain the CCDFs of time lapse Δt under different driving velocities. Figure 12(a) shows that the distribution has a power-law tail and the power-law exponent increases slightly with the increase of the driving velocity, but not larger than 2, indicating that the system always tends to clog within the range of the driving velocity. With $V_{\text{belt}} = 2$ cm/s, the minimum time lapse Δt_c is about 1 s, which is the largest of all driving velocities studied. We also calculate the mean flow rate for different driving velocities, and the maximum Δt_c is about 0.6 s when the mean flow rate becomes stable, as shown in Fig. 12(b). Here we adopt $\Delta t_c = 1$ s as the minimum time lapse to distinguish clog from flow.

Figure 13(a) shows that all rescaled avalanche sizes overlap to form a single exponential curve. Figure 13(b) shows the dependence of clogging probability $J_N(v)$ on the driving velocity V_{belt} under different N . The clogging probability decreases with the increase of the driving velocity, and finally approaches saturation. With the increase of N , $J_N(v)$ gradually tends to be a horizontal line.

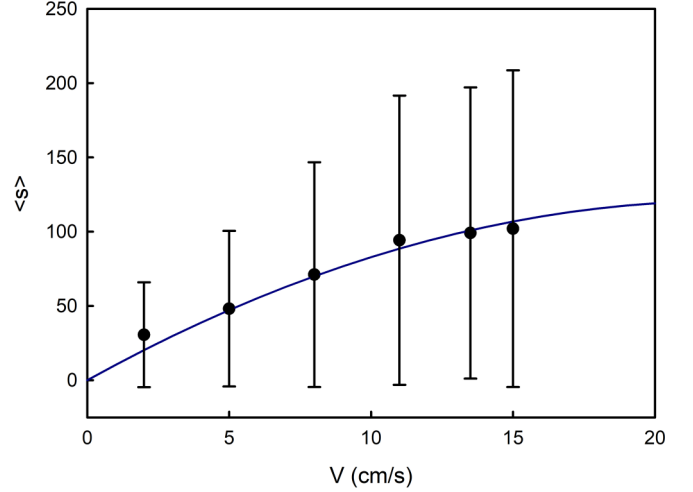


FIG. 14. The average avalanche size as a function of the driving velocity. The solid line is the fit from Eq. (4). The fitting parameters are $a = 346.5(\text{cm/s})^{-1}$, $b = -335.9(\text{cm/s})^{-1}$, and $c = -6.87 \times 10^{-4}(\text{cm/s})^{-1}$.

The experimental results show that the average avalanche size $\langle s \rangle$ monotonically increases with the driving velocity V_{belt} ; see Fig. 14. The quantitative relationship between $\langle s \rangle$ and V_{belt} determines the mathematical expression of $J_N(v)$. The driving velocity V_{belt} has two effects on the motion of the particles near the outlet. We made a conjecture to estimate the relationship.

On one side, with the increase of V_{belt} , the blocking probability $1 - p$ monotonically decreases until it is finally saturated, as shown in Fig. 16. The mean flowing time ΔT between two clogging events could be closely related to the blocking probability of a particle at the outlet. Qualitatively speaking, the mean flowing time ΔT is supposed to be inversely proportional to the blocking probability $1 - p$. That is to say, ΔT may increase with V_{belt} , and finally reach saturation. Based on the simple assumption, we propose an

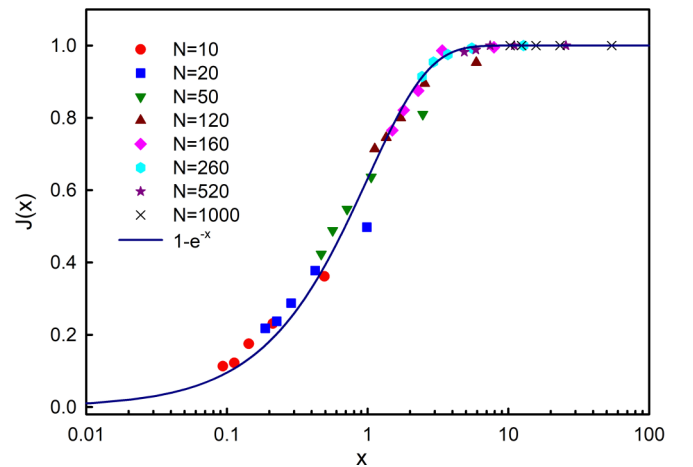


FIG. 15. The clogging probability J as a function of the scaled variable $x = -N/(aV_{\text{belt}} + bV_{\text{belt}}e^{-cV_{\text{belt}}})$. The experimental data from different driving velocity and N collapse into the theoretical curve $1 - e^{-x}$.

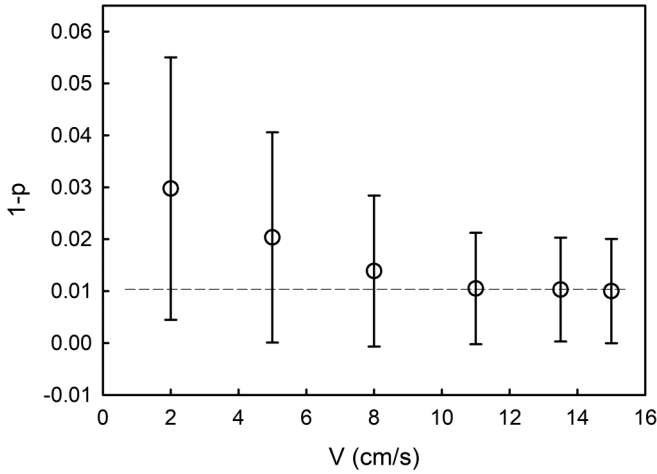


FIG. 16. The blocking probability of a particle at the outlet, $1-p$, as a function of the driving velocity ($D = 4.0$, and $\theta=0^\circ$).

empirical expression to describe the relation between ΔT and V_{belt} : $\Delta T = a_1 - a_2 e^{-bV_{\text{belt}}}$; a_1 and a_2 are fitting parameters.

In the other aspect, with the increase of the driving velocity V_{belt} , the particle velocity near the outlet increases correspondingly. We propose a linear ansatz: The velocity of particles discharging through the outlet increases linearly with the driving velocity V_{belt} . Namely, $V_{\text{particle}} = kV_{\text{belt}}$; k is a proportional parameter. As stated previously, the average avalanche size is the average number of particles discharging out of the outlet between two consecutive clogging events, which is the product of the mean flowing time ΔT between two clogging events and the velocity of particles discharging through the outlet V_{particle} . Thus,

$$\langle s \rangle = aV_{\text{belt}} + bV_{\text{belt}}e^{-cV_{\text{belt}}}. \quad (4)$$

The agreement with the experimental data is proving the validity of the proposed Eq. (4); see Fig. 14.

Inserting Eq. (4) into $J_N(D) = 1 - \exp(-N/\langle s \rangle)$, we obtain

$$J_N(V_{\text{belt}}) = 1 - \exp[-N/(aV_{\text{belt}} + bV_{\text{belt}}e^{-cV_{\text{belt}}})]. \quad (5)$$

Letting $x = -N/(aV_{\text{belt}} + bV_{\text{belt}}e^{-cV_{\text{belt}}})$, all experimental data collapse into a single curve presented by Eq. (5), as shown in Fig. 15.

With the analysis of Figs. 12(a), 13(b), 14, and 16, now we can answer the question raised at the beginning of this section. The system of horizontal hopper flow driven by a conveyor belt does not show the fast is slow effect that is common in the sheep, robots, crowd, and traffic flow. Instead, the clogging tends to be weakened in the system by the increase of the driving velocity, suggesting a possible fast is fast behavior, which is similar to the phenomenon in the evacuation of an extremely panicked crowd from the emergency exit simulated by the social force model [33]. In this reference, the force balance model points out that particles in a clogging arch are subjected to pushing force and frictional force. The pushing force is proportional to the desired velocity of particles (in our experiment, the desired velocity is the driving velocity), and the frictional force is linearly proportional to the particle's

actual velocity and the compression between the individuals in the clogging arch. If the two forces are balanced, the clogging arch will remain stable. As the pushing force in the crowd increases with the desired velocity, the compression between individuals in the clogging arch seems not enough to provide a slowing down in the moving pedestrian. The clogging arch will be broken soon. Thus, a “faster is faster” effect appears. The fast is fast behavior in our experiment could be the case. In our experiment, we increase the desired velocity (driving velocity) by an order of magnitude from 2 to 15 cm/s. The pushing force is greatly increased. The particles used in the experiment are hard plastic disks; it is very difficult to cause compression between individuals. The frictional force due to the compression may not catch up with the increase of the pushing force.

In addition, compared with the geometric effect (outlet size and hopper angle) on the clogging in the horizontal flow driven by a conveyor belt, the kinematic effect (driving velocity) is much weaker. For the geometric effect, the system eventually switches a clogging state to a flowing state, whether the outlet size is increased or the hopper angle is enlarged. For example, when the outlet size is doubled, increasing from $D = 3.0$ to $D = 6.0$, the blocking probability $1-p$ is reduced by about two orders of magnitude, resulting in the transition from a clogging state to a flowing state. When the driving velocity nearly increases by an order of magnitude (from 2 to 15 cm/s), the blocking probability $1-p$ is only reduced by three times and the power exponent α is still less than 2, implying that the system possibly tends to be in the clogging state. This suggests that the geometric effects play a more critical role in determining the clogging characteristics in the case of the conveyor system.

IV. CONCLUSION

In conclusion, due to the independence of the driving velocity on the outlet size, separating geometrical and kinematic contributions to the clogging process becomes possible for horizontal hopper flow driven by a conveyor belt. We experimentally investigate the geometric and kinematic effects on the clogging and flowing process in such a horizontal hopper flow, respectively. By enlarging the outlet size or increasing the hopper angle, we find that the clogging state can switch to the flowing state, and the blocking probability of a particle near the outlet can be reduced by almost two orders of magnitude. A model from the gravity-driven hopper clogging describes the dependence of clogging probability on the outlet size and hopper angle in horizontal hopper flow, which suggests that some underlying mechanisms could be common in clogging issues in the two systems.

Besides, we do not find the fast is slow effect, which is common in other horizontal flow, within the range of driving velocity in our investigation. Instead, a possible fast is fast behavior is shown in the conveyor belt system. We speculate that the effect could originate from the force imbalance in the blocking arch. Specifically, the frictional force due to the compression between particles cannot catch up with the

increase of the pushing force that is closely related to the driving velocity, which enables the arch to be more likely to be broken. Finally, by comparing the parameters describing the clogging characteristics, such as the power-law exponent, average avalanche size, and so on, we find that the geometric effect more effectively affects the clogging in the conveyor belt system.

ACKNOWLEDGMENTS

This work was supported by the National Natural Science Foundation of China (Grant No. 11974044) and National Key Research and Development Program of China (Program No. 2016YFC1401001). We appreciate J. P. Johnson for a critical reading of this paper.

-
- [1] D. Helbing, I. Farkas, and T. Vicsek, *Nature (London, UK)* **407**, 487 (2000).
 - [2] K. To, P.-Y. Lai, and H. K. Pak, *Phys. Rev. Lett.* **86**, 71 (2001).
 - [3] R. Zhou and H.-C. Chang, *J. Colloid Interface Sci.* **287**, 647 (2005).
 - [4] A. Bricard, J.-B. Caussin, N. Desreumaux, O. Dauchot, and D. Bartolo, *Nature* **503**, 95 (2013).
 - [5] T. Masuda, K. Nishinari, and A. Schadschneider, *Phys. Rev. Lett.* **112**, 138701 (2014).
 - [6] S. Saraf and S. V. Franklin, *Phys. Rev. E* **83**, 030301(R) (2011).
 - [7] C. C. Thomas and D. J. Durian, *Phys. Rev. E* **87**, 052201 (2013).
 - [8] A. Ashour, S. Wegner, T. Trittel, T. Börzsönyi, and R. Stannarius, *Soft Matter* **13**, 402 (2017).
 - [9] J. Tang and R. P. Behringer, *Europhys. Lett.* **114**, 34002 (2016).
 - [10] A. Ashour, T. Trittel, T. Börzsönyi, and R. Stannarius, *Phys. Rev. Fluids* **2**, 123302 (2017).
 - [11] K. Endo, K. A. Reddy, and H. Katsuragi, *Phys. Rev. Fluids* **2**, 094302 (2017).
 - [12] I. Zuriguel, A. Janda, A. Garcimartín, C. Lozano, R. Arévalo, and D. Maza, *Phys. Rev. Lett.* **107**, 278001 (2011).
 - [13] C. Lozano, A. Janda, A. Garcimartín, D. Maza, and I. Zuriguel, *Phys. Rev. E* **86**, 031306 (2012).
 - [14] J. Koivisto and D. J. Durian, *Phys. Rev. E* **95**, 032904 (2017).
 - [15] J. Koivisto, M. Korhonen, M. Alava, C. P. Ortiz, D. J. Durian, and A. Puisto, *Soft Matter* **13**, 7657 (2017).
 - [16] R. Arévalo and I. Zuriguel, *Soft Matter* **12**, 123 (2016).
 - [17] H. G. Sheldon and D. J. Durian, *Granul. Matter* **12**, 579 (2010).
 - [18] D. Gella, I. Zuriguel, and D. Maza, *Phys. Rev. Lett.* **121**, 138001 (2018).
 - [19] M. A. Aguirre, J. G. Grande, A. Calvo, L. A. Pugnaloni, and J.-C. Géminard, *Phys. Rev. Lett.* **104**, 238002 (2010).
 - [20] A. Garcimartín, J. M. Pastor, L. M. Ferrer, J. J. Ramos, C. Martín-Gómez, and I. Zuriguel, *Phys. Rev. E* **91**, 022808 (2015).
 - [21] G. A. Patterson, P. I. Fierens, F. Sangiuliano Jimka, P. G. König, A. Garcimartín, I. Zuriguel, L. A. Pugnaloni, and D. R. Parisi, *Phys. Rev. Lett.* **119**, 248301 (2017).
 - [22] I. Zuriguel, D. R. Parisi, R. C. Hidalgo, C. Lozano, A. Janda, P. A. Gago, J. P. Peralta, L. M. Ferrer, L. A. Pugnaloni, E. Clément, D. Maza, I. Pagonabarraga, and A. Garcimartín, *Sci. Rep.* **4**, 7324 (2014).
 - [23] J. M. Pastor, A. Garcimartín, P. A. Gago, J. P. Peralta, C. Martín-Gómez, L. M. Ferrer, D. Maza, D. R. Parisi, L. A. Pugnaloni, and I. Zuriguel, *Phys. Rev. E* **92**, 062817 (2015).
 - [24] A. Clauset, C. R. Shalizi, and M. E. J. Newman, *SIAM Rev.* **51**, 661 (2009).
 - [25] I. Zuriguel, A. Garcimartín, D. Maza, L. A. Pugnaloni, and J. M. Pastor, *Phys. Rev. E* **71**, 051303 (2005).
 - [26] A. Janda, I. Zuriguel, A. Garcimartín, L. A. Pugnaloni, and D. Maza, *EPL* **84**, 44002 (2008).
 - [27] K. To, *Phys. Rev. E* **71**, 060301(R) (2005).
 - [28] D. López-Rodríguez, D. Gella, K. To, D. Maza, A. Garcimartín, and I. Zuriguel, *Phys. Rev. E* **99**, 032901 (2019).
 - [29] M. Benyammine, P. Aussillous, and D. B. Dalloz, *EPJ Web Conf.* **140**, 03043 (2017).
 - [30] X. Wang, H.-W. Zhu, Q.-F. Shi, and N. Zheng, *Chin. Phys. B* **29**, 044502 (2020).
 - [31] T. Nagatani, *Rep. Prog. Phys.* **65**, 1331 (2002).
 - [32] M. Haghani and M. Sarvi, *Transp. Res. Part B: Methodol.* **107**, 253 (2018).
 - [33] I. M. Sticco, F. E. Cornes, G. A. Frank, and C. O. Dorso, *Phys. Rev. E* **96**, 052303 (2017).